Fabrication of Au functionalized TiO2 nanofibers for photocatalytic application

Xiaojiao Yang, Vincent Salles, Mathieu Maillard, Yusuf Valentino Kaneti, Minsu Liu, Catherine Journet, Xuchuan Jiang, Ying Liu, Arnaud Brioude

J Nanopart Res (2019) 21: 160
https://doi.org/10.1007/s11051-019-4600-8

RESEARCH PAPER

Fabrication of Au functionalized TiO_2 nanofibers for photocatalytic application

Xiaojiao Yang · Vincent Salles · Mathieu Maillard · Yusuf Valentino Kaneti · Minsu Liu · Catherine Journet · Xuchuan Jiang · Ying Liu · Arnaud Brioude

Received: 2 April 2019 / Accepted: 2 July 2019 / Published online: 17 July 2019

Abstract Pristine titanium dioxide (TiO_2) and gold (Au)-doped TiO_2 (TiO_2–Au) composite nanofibers (NFs) with different Au contents were fabricated by electrospinning. The thermal behavior of the as-spun composite precursor NFs were analyzed and characterized. Photocatalytic reactions were performed with methyl blue (MB) aqueous solution under UV–Vis and different irradiation wavelengths (including 360 nm, 528 nm, and 360 nm and 528 nm together). As a result, the morphology and the structure of TiO_2–Au composite NFs were significantly influenced by calcination temperature, leading to the controllable phase ratio of anatase and rutile in TiO_2. TiO_2–Au composite NFs, with an average diameter of 171 nm containing Au crystals of about 10 nm, exhibited enhanced photocatalytic efficiency toward the MB, compared to that of commercial P25 (a multiphase TiO_2 98% anatase and 2% rutile). The corresponding degradation level reached 95% after 10 min. When irradiated with light having different wavelengths, the TiO_2–Au composite NFs catalyst had the best performance under 360 nm and 528 nm together, indicating that Au NPs functionalized TiO_2 NFs can enhance the photocatalysis from UV range to visible range. The mechanism of photocatalytic reactions under different irradiations is discussed in the present paper.

Keywords TiO_2 · Au · Functionalized · Photocatalysis · Nanofiber · Nanostructured catalysts

Electronic supplementary material The online version of this article (https://doi.org/10.1007/s11051-019-4600-8) contains supplementary material, which is available to authorized users.

X. Yang · Y. Liu (✉)
College of Materials Science and Engineering, Sichuan University, No.24 South Section 1, Yihuan Road, Chengdu 610065, People's Republic of China
e-mail: liuying5536@scu.edu.cn

V. Salles · M. Maillard · C. Journet · A. Brioude (✉)
Univ Lyon, Université Claude Bernard Lyon 1, CNRS, Laboratoire des Multimatériaux et Interfaces, F-69622 Villeurbanne, France
e-mail: arnaud.brioude@univ-lyon1.fr

Y. V. Kaneti · M. Liu · X. Jiang
Department of Chemical Engineering, Monash University, Melbourne, VIC 3800, Australia

Introduction

Titanium dioxide (TiO_2)–based materials have attracted significant attention for photocatalysis because of their unique photocatalytic properties (Chen et al. 2011), combined with long-term stability, strong oxidizing ability, abundance, low cost, and nontoxic properties. By means of light irradiation, they can induce a wide range of chemical reactions, including the oxidation of organic pollutants for water purification (Lang et al. 2014; Mushtaq et al. 2016), air purification (Lyulyukin et al. 2018), water splitting (Butburee et al. 2018), and sterilization (Ho et al. 2004) applications. However, the application of TiO_2-based materials in water purification area still has some limitations. Because of the wide bandgap (~ 3.2 eV) of TiO_2, it can only absorb UV light

(< 380 nm wavelength). As a consequence, it exhibits a very low solar light harvesting efficiency without additional materials and thus limiting expected oxidation reactions (Xing et al. 2018). Besides, such reactions are also dependent on the recombination rate of photo-excited electron-hole (e^-/h^+) pairs that the rapid recombination of photogenerated charge carriers may decrease the photocatalytic efficiency as well (Fazio et al. 2016). Meanwhile, the recycling use of common TiO_2 catalyst is also made difficult by the small size of nanoparticles (NPs) (Fazio et al. 2016). Therefore, the development of more efficient TiO_2-based photocatalysts remains challenging, by combining efficiency and management of NPs-based materials.

The mixed phases of anatase and rutile for TiO_2 have been reported to exhibit higher activities involving photo-excited charges migration between these two phases (Tsukamoto et al. 2012), which enhances in return the charge separation. Although the mechanism is not fully understood, the photocatalytic efficiency of TiO_2 materials has crystallite phase-dependent synergistic effect. TiO_2 nanofibers (NFs) have shown various significant advantages as they connect the nano- and microworld having specific morphology with diameters in nanoscale and lengths ranging from a few hundreds of nanometers to several meters (Li and Xia 2003). This specific morphology prolonging life of electron-hole pairs, no aggregation in water, and easy separation, thus it is easy to recycle without any complicated procedures compared to the use of NPs (Wang et al. 2018). And also, the NFs propose the possibility to fabricate flexible film photocatalyst. Electrospinning (ES) is one of the simplest and most versatile techniques to fabricate a wide range of suitable NFs with high production efficiency (Greiner and Wendorff 2007). In addition, expanding the photoresponse of TiO_2 to the visible range for enhancing solar light harvesting has been an intense research recently. As such, loading TiO_2 photocatalyst with noble metal(s), especially with Au as a cocatalyst (Su et al. 2012), has been considered as one of the most promising catalysts for photocatalytic reactions. The Au NPs act as an electron sink and active reaction sites for photocatalytic reactions (Sridhar et al. 2018; Yang and Mou 2018; Moretti et al. 2018). Thus, TiO_2–Au composite NFs extend the absorption range from UV to visible range and reduce the recombination rate of e^-/h^+ pairs.

This work is focused on TiO_2–Au composite NFs fabricated by the ES process. The gold (Au) content and its dispersion inside TiO_2–Au composite NFs are controllable by the ES process at a molecular level. Besides, the phase structures of TiO_2, morphology, particle size, and specific surface area of TiO_2–Au composite NFs are tuned by the calcination temperature (Online et al. 2014). Thermal behavior of as-spun composite NFs, influence of Au contents, effect of calcination temperature on morphology, phase structures, and particle size of TiO_2 in NFs were investigated. Meanwhile, TiO_2–Au composite NFs having various Au contents were fabricated and the morphology, structure, and crystallite size of both Au and titania were also analyzed. The TiO_2 NFs obtained from different calcination temperatures and the TiO_2–Au composite NFs with different Au contents were then used as catalysts for the degradation of methyl blue (MB), as a case study, in aqueous solution under UV irradiation. In order to have a better understanding of the photocatalytic mechanisms, irradiation with different wavelengths of 360 nm (in UV range), 528 nm (in visible range), and combining 360 nm and 528 nm together were chosen as the typical wavelengths for comparison experiments.

Experimental section

Fabrication of TiO_2 and TiO_2–Au composite NFs

In a typical procedure, 7 g of polyvinylpyrrolidone (PVP, Aldrich, Mw ~ 1,300,000) was dissolved in 93 g of ethanol (EtOH) and then stirred at room temperature for 12 h, to obtain the homogenous PVP–EtOH solution with 7 wt% of PVP. Then 1.5 g of titanium isopropoxide (TTIP, $C_{12}H_{28}O_4Ti$, ≥ 99.9%, Sigma Aldrich) was added into a mixture of acetic acid (3 mL) and EtOH (3 mL) to form the TTIP solution. The TTIP solution was subsequently mixed with 6.43 g of PVP–EtOH solution. To ensure good mixture homogeneity, the resulting solution was then stirred at room temperature for 2 h. After a typical ES process, the as-spun PVP–TTIP composite NFs were obtained and calcined in air for 2 h at different temperatures of 500 °C, 600 °C, 700 °C, and 800 °C, and then the samples of TiO_2 NFs were obtained and noted as follows: TiO_2—500 °C, TiO_2—600 °C, TiO_2—700 °C, and TiO_2—800 °C, respectively.

To prepare TiO_2–Au composite NFs, Au precursor ($HAuCl_4 \cdot 3H_2O$, ≥ 99.9%, Sigma Aldrich) with an amount of 50 mg, 75 mg, and 150 mg was dissolved

in the raw PVP–TTIP solution before ES. The as-obtained filaments were then thermally treated at 500 °C in air for 2 h to obtain the TiO_2–Au NFs. The samples TiO_2–Au with different Au contents were named as TiO_2–Au—2 wt%, TiO_2–Au—4 wt%, and TiO_2–Au—8 wt%, respectively. In the following, pristine TiO_2 NFs is named as TiO_2–Au—0 wt% and that is equal to TiO_2—500 °C.

In a typical ES process (Fig. 1), the ES solution was loaded into a plastic syringe equipped with a 21-gauge stainless steel needle, whose tip was connected to a high-voltage power supply (HV supply from Iseg Co., T1CP 300 304 p). The distance between the needle tip and the grounded collector (covered with an aluminum foil) was placed at 15 cm. A continuous feeding rate of 1.5 mL h^{-1} was controlled with a syringe pump (KDS–100, Bioseb Co.). Under these working conditions, an electric field of 0.8 kV cm^{-1} led to a stable jet. The composite as-spun NFs were collected onto the aluminum foil for 6 h before being peeled off and calcined.

Characterization

In order to analyze the thermal behavior of as-spun PVP–TTIP–Au composite NFs, the pure PVP, PVP–Au, and PVP–TTIP NFs were fabricated, keeping the same proportion of each component with the sample of PVP–TTIP–Au NFs (Au content of 8 wt%). Thermogravimetric analysis (TGA/SDTA 851, Mettler Toledo, 30–800 °C, at 3 °C·min^{-1}, in air) probed the thermal decomposition of the studied compounds. TiO_2 NFs and TiO_2–Au composite NFs were characterized using scanning electron microscopy (SEM, FEI Guanta 250) and high-resolution transmission electron microscopy (HRTEM, JEOL 2100F) with an accelerating voltage of 200 kV. The formation of titania and Au crystals with the temperature was characterized by X-ray diffraction (XRD, Phillips, PW 1830/40 wide-angle goniometer using Cu Kα 1 $\lambda = 1.54056$ Å) from 10° to 90° in 2θ. The average crystal sizes of titania and Au were determined using the three intensest peaks of XRD from each sample using Scherrer's equation (Bian et al. 2014). N_2 adsorption-desorption isotherms for TiO_2 NFs and TiO_2–Au NFs were carried out using a Sorptomatic system (Thermo Electron Corporation) and their surface areas have been measured by BET (Brunauer-Emmett-Teller) equation. The Au content in TiO_2–Au samples was determined by inductively coupled plasma optical emission spectrometry (ICP–OES, Varian, Vista–MPX). The main diameter of NFs and the average size of Au NPs were determined for each sample from measurements on SEM images performed on 100 filaments using the software of NanoMeasurer.

Photocatalytic activity

The photocatalytic activities of the samples were determined by measuring the degradation of methyl blue (MB) under different wavelengths of irradiation (360 nm, 528 nm, and combining UV and visible together at 360 nm and 528 nm) in a reactor. For UV irradiation, a 150 W UVA light was set in the center of the reactor. The luminance of the light source over the reactant solution was 0.7 W cm^{-2} for a surface of 214 cm^2 and the total irradiation time was 40 min. A 100-mL solution of 30 ppm dye was injected into the reactor, containing 20 mg of the photocatalyst, well-dispersed using an ultrasonic bath. Then the suspension

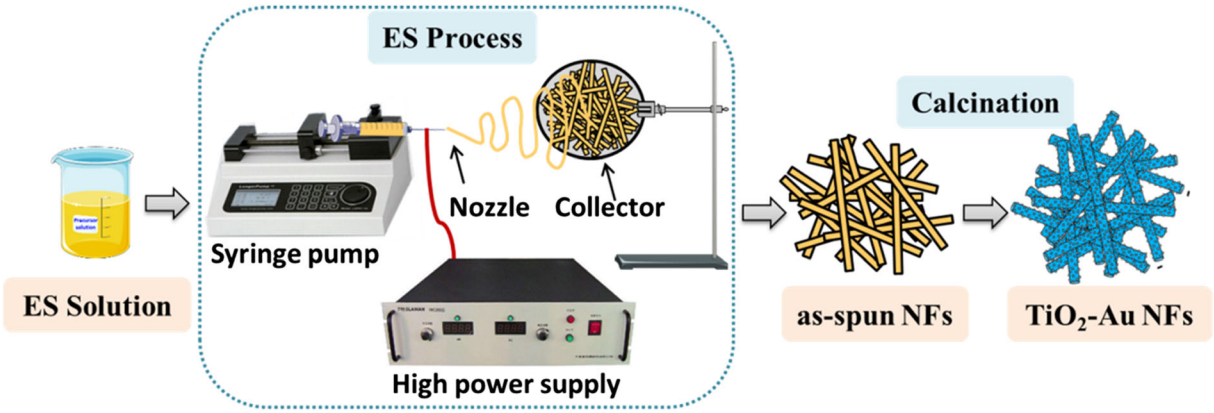

Fig. 1 Schematic diagram of synthesis process of TiO_2–Au composite NFs

was stirred for 30 min in the dark to achieve the adsorption-desorption equilibrium. For the different wavelengths of irradiation, a rectangular quartz cuvette was used as the reactor, and the lamps were set in front of the reactor. The solution of 30 ppm dyes with the same concentration of photocatalyst was injected into the reaction system. After degradation, the supernatant of the solution was obtained via centrifugation (Eppendorf, 5810) to separate the catalysts and the solution. The supernatant was then characterized after a suitable dilution by UV–Vis spectroscopy (SAFAS, Monaco, UV mc^2), recorded from 400 to 800 nm with a 2-nm step and 0.1 s of integration time.

Results and discussion

Thermal behavior of precursor NFs

In order to understand the thermal behavior of PVP–TTIP–Au composite NFs during the whole calcination process, pure PVP, PVP–Au, PVP–TTIP, and PVP–TTIP–Au composite NFs were analyzed by TGA. The decomposition of these four samples ended at different temperatures according to the TGA curves. For pure PVP NFs (Fig. 2d), the final decomposition temperature was 650 °C with a remaining weight of 1.1%, assumed to be a residue of carbon. Keeping the same related ratio of Au or titania to PVP, the final decomposition temperature shifted from 650 °C toward lower temperature 440 °C for PVP–Au, 500 °C for PVP–TTIP, and 420 °C for PVP–TTIP–Au. These temperature variations reflect the oxidizing capability of the Au and titania precursors. Thus, by introducing metal sources, it can influence the final decomposition temperature of the metal/polymer composites. The final weight% reflects the amount of non-volatile inorganic compound–like metallic Au and titania and the mixture of both. It can also be seen on curves (a) and (b) of Fig. 2 that there is still a small weight loss at 700 °C, while the curves of (c) and (d) for PVP–Au and PVP are flat. This small weight loss possibly may be attributed to the reduction between the residual carbon and TiO_2. Thus, the calcination temperatures to obtain the final products of TiO_2 NFs were chosen at 500 °C, 600 °C, 700 °C, and 800 °C, depending on the precursor composition whereas for TiO_2–Au–4 wt% NFs. The calcination temperature was fixed at 500 °C.

Temperature effect on morphology and composition of TiO_2 NFs

The calcination temperature plays an important role in the morphology and the compositions of the final products. To obtain pristine TiO_2 NFs, different calcination temperatures from 500 to 800 °C in the air were studied on the as-spun PVP–TTIP NFs (Fig. 3a–d). The average diameter of the samples was 164 nm, 119 nm, 112 nm,

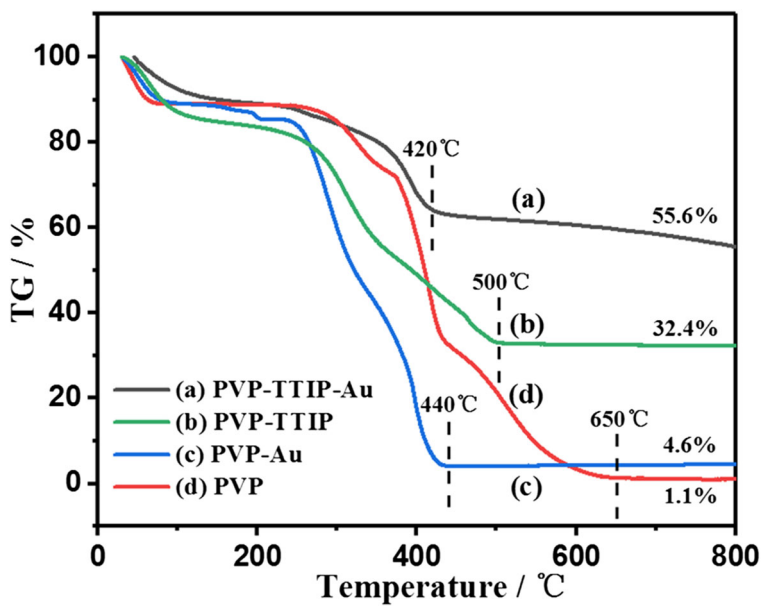

Fig. 2 TG curves of composite NFs calcined under air atmosphere: (**a**) PVP–TTIP–Au, (**b**) PVP–TTIP, (**c**) PVP–Au, and (**d**) PVP

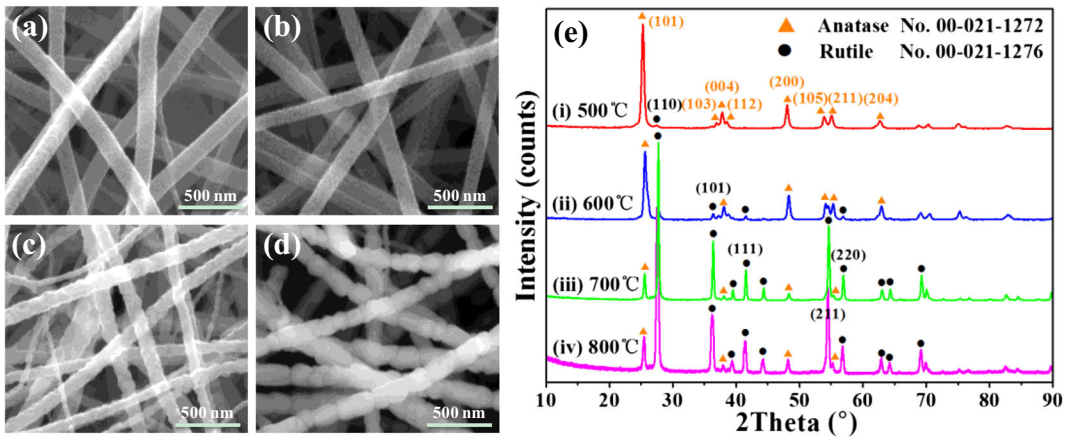

Fig. 3 SEM images of TiO_2 NFs with different calcination temperatures: **a** 500 °C, **b** 600 °C, **c** 700 °C, **d** 800 °C, and **e** XRD patterns of TiO_2 NFs obtained with different calcination temperatures

and 137 nm, while annealed at 500 °C, 600 °C, 700 °C, and 800 °C respectively, as shown in Table 1. It is assumed that the decomposition of PVP polymer at 500 °C creates porous fibers made of small TiO_2 NPs (Fig. 3a). As the temperature increased to 600 °C, the diameter of the porous fibers shrunk to 119 nm, probably due to a sintering mechanism between the titania particles (Hahn et al. 1990).

Comparing the samples obtained at 600 °C and 700 °C, the fiber diameter had no obvious change but the surface roughness increased accordingly to the sintering of NPs. When the calcination temperature reached 800 °C, TiO_2 NFs were made of a linear assembly of large TiO_2 particles with a typical necklace shape. The mean NFs diameter of 137 nm at 800 °C is larger than the one of the NFs obtained at lower temperature (119 nm at 600 °C and 112 nm at 700 °C).

The crystal structures of pristine TiO_2 samples were determined by XRD. Figure 3e displays XRD patterns of TiO_2 NFs samples calcined in the 500–800 °C temperature range. The XRD pattern of TiO_2—500 °C can be well-assigned to anatase (JCPDS Card No. 00–021–1272), with lattice parameters $a = 3.7852$ Å, $b = 3.7852$ Å, and $c = 9.5139$ Å. Peaks at $2\theta = 25.3°$, 37.8°, and 48.1° can be indexed to the (101), (004), and (200) planes of anatase, respectively. When carefully checking, a small peak could be found at 27.4°, which was attributed to the (110) planes of rutile (JCPDS Card No. 00–021–1276). As the temperature increased to 600 °C, new peaks appeared at $2\theta = 27.4°$, 36.1°, 41.2°, and 56.6°, indexed as the (110), (101), (111), and (220) planes of rutile, respectively. The component of anatase decreased and rutile increased as the temperature is rising from 700 to 800 °C. The average crystal sizes of TiO_2 were 27 nm, 21 nm, 27 nm, and 22 nm for samples obtained from 500 °C, 600 °C, 700 °C, and 800 °C, respectively. There was no obvious change in the crystalline size of TiO_2 by increasing the temperature. The intensity of anatase main peak decreased and that of rutile increased while the temperature increased, indicating a diminution of the anatase/rutile ratio.

Table 1 Average diameter, crystallite size, and anatase/rutile phase ratio of TiO_2 obtained from different calcination temperatures

TiO_2 sample	Average diameter/nm	Crystallite size/nm	Anatase:rutile/ %	R (%)
500 °C	164 ± 21	27	98:2	3%
600 °C	119 ± 13	21	84:16	11%
700 °C	112 ± 17	27	13:87	77%
800 °C	137 ± 18	22	12:88	82%

In order to analyze the anatase/rutile ratio of TiO_2 NFs obtained from different calcination temperatures, the Rietveld refinement analysis based on the XRD data was performed by the Brass software. Temperature is one of the key factors to form different structures and phases. TiO_2 has three different phases of anatase, rutile, and brookite (Dambournet et al. 2010). The commercial TiO_2 (P25) is composed of anatase and rutile with the ratio of 81:19 (Han et al. 2018). The ratio of anatase to rutile is 98:2 at 500 °C, corresponding to almost pure anatase at this temperature, whereas rutile content gradually increases with calcination temperature, up to 88% at 800 °C (as listed in Table 1). The percent content of

rutile TiO_2 (R (%)) is calculated by means of the equation $R\ (\%) = 0.79(I_R/I_A)/(1 + 0.79(I_R/I_A))$ (Wang et al. 2018), where I_A and I_R are the intensities for TiO_2 anatase and rutile phase. R (%) values were calculated to be 3%, 11%, 77%, and 82% for 500 °C, 600 °C, 700 °C, and 800 °C, respectively. Both results of the calculation by the Brass software or the equation of R (%) are consistent with the fact that anatase is thermodynamically the most stable phase at low temperature, but not at high temperature. Hence, by modifying the calcination temperature, it is a good way to adjust the ratio of anatase to rutile phase in titania fibers.

Au content effects on morphology and composition of TiO_2–Au composite NFs

Au contents in the TiO_2–Au composite NFs measured by ICP are 2.02%, 4.32%, and 7.99% in weight, as listed in Table 2. Thus, the corresponding sample names were set as follows: 2 wt%, 4 wt%, and 8 wt%, respectively. Compared to the calculated results based on the initial weight of Ti and Au precursors of 5.6%, 8.2%, and 15.1%, the contents from ICP results were almost two times lower. This might be due to the sample preparation process for ICP experiments. During the ES process, Au ions were indeed present into the as-spun composite NFs and homogeneously dispersed at a molecular level (Shim et al. 2016). After thermal treatment, TiO_2–Au composite NFs were obtained and then put into aqua regia in order to dissolve Au NPs. Since those NPs were not percolated, it is easy to consider that the dissolution of the Au NPs is only possible for those localized at the surface. The centrifugation step could not split the composite as finely as it would have been necessary to render possible the dissolution of all the particles. As a result, the Au NPs embedded inside the TiO_2 matrix remained solid and were not taken into account by the ICP dosage. However, the authors of the present study decided to take into account the Au amount practically measured and not the theoretical and expected one.

The morphology of Au-containing NFs was studied by SEM and TEM (Fig. 4a–e). All the samples have a fibrous morphology and contain homogenously dispersed bright dots, identified to be Au NPs. The average diameter of samples with Au contents of 2 wt% (169 nm) and 4 wt% (171 nm) are very close to that of pristine TiO_2 NFs (164 nm). For higher Au concentration (8 wt%), the diameter decreases drastically because it modifies the relative proportion of TTIP precursor and polymer, thus modifies the ES solution ionic strength and rheological properties. It is therefore likely to modify the ES conditions and the fiber diameter consequently. From TEM and HR-TEM images of the sample containing 4 wt% of Au (Fig. 4d, e), it is possible to conclude that the TiO_2 and Au domains are small and well crystallized. The sample presents a strong homogeneity with a very good dispersion of 10 nm Au NPs at the surface and inside the TiO_2 NFs matrix.

The crystal structures of TiO_2–Au composite NFs were determined by XRD (Fig. 4f). For TiO_2–Au—0 wt%, the pristine TiO_2 XRD pattern was easily attributed to anatase phase (JCPDS Card No. 00–021–1272), as previously discussed in this paper. When Au was introduced in the filaments up to 2 wt%, two additional peaks centered at $2\theta = 44.4°$ and 64.6° were observed, corresponding to the (200) and (220) planes of the Au cubic phase (JCPDS Card No.00–004–0784). By increasing this Au amount to 4 wt%, the two peaks at $2\theta = 36.9°$ and 38.6°, corresponding to the (103) and (112) planes of anatase (JCPDS Card No. 00–021–1272) were mixed with the strong peak at $2\theta = 38.2°$ from the (111) planes from Au.

The average size of Au NPs in the three samples is 10.0 nm (TiO_2–Au—2 wt%), 9.8 nm (TiO_2–Au—4 wt%), and 9.3 nm (TiO_2–Au—8 wt%), respectively. This uniform size of Au NPs benefits from the in situ

Table 2 Au content, average fiber diameter, Au NPs size, and crystallite size of TiO_2–Au composite NFs obtained from different Au concentrations

TiO_2–Au sample	Au contents/wt%		Fiber diameter nm	NPs size Au/nm	Crystallite size/nm	
	ICP	Calculation			TiO_2	Au
2 wt%	2.0	5.6	169 ± 39	10.0 ± 2.2	34	8
4 wt%	4.3	8.2	171 ± 31	9.8 ± 2.6	19	8
8 wt%	8.0	15.1	130 ± 20	9.3 ± 1.8	18	11

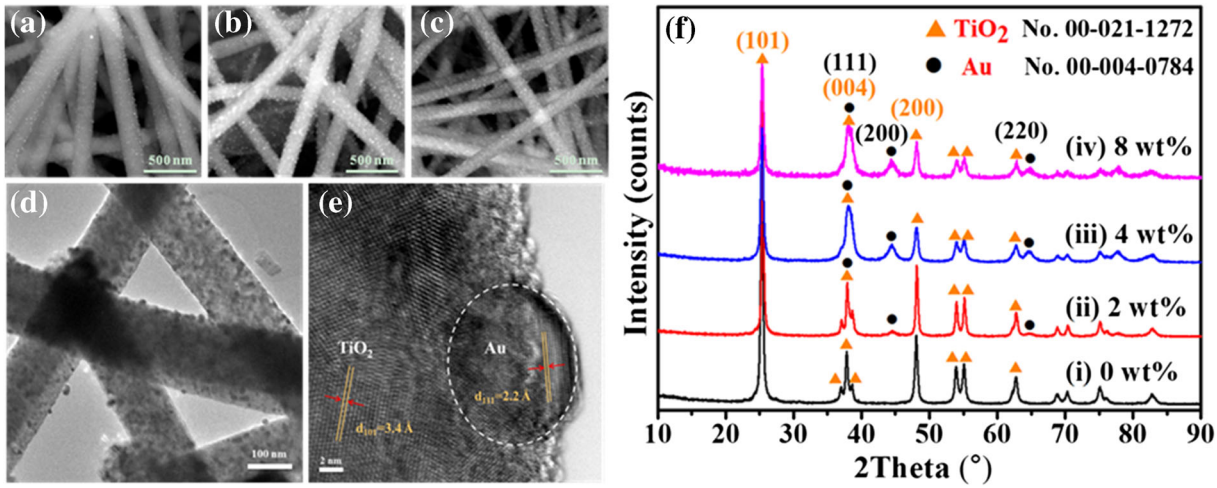

Fig. 4 SEM images of TiO_2–Au composite NFs with different Au contents at 500 °C: **a** 2 wt%, **b** 4 wt%, **c** 8 wt%, **d** TEM, and **e** HR–TEM images of TiO_2–Au–4 wt%; **f** XRD patterns of TiO_2–Au composite NFs with different Au contents

reduction of Au ions to form Au NPs at low temperature before the formation of TiO_2 crystallites (Conceicao and Vieira Ferreira 2018). The reduction mechanism is likely due to the oxidation of terminal hydroxyl groups from PVP as observed in hydrothermal synthesis of Au NPs (Xiong et al. 2006) or directly oxidation of the polymer backbone at high temperature, due to the high redox potential of $HAuCl_4$ ($E^0 = 0.93$ V/ENH at 298 K) (Yan et al. 2010). The PVP before ES plays an important role to prevent the Au NPs aggregation (Wang et al. 2018). According to the literature, ES and subsequent calcination provide a single-step elaboration to allow the noble metal NPs loading with size control in TiO_2 NFs. As a carrier polymer, PVP is primordial for the development of monodisperse supported noble metal nanocrystals, and the presence of well-dispersed noble NPs is ascribed to the protecting role of PVP at the surface of the nascent nanoclusters to the calcination step following ES of the composite NFs (Cavaliere et al. 2011). The Au contents in the final sample can be varied by the concentration and volume of Au aqueous solution added into the ES solution. The crystallite size of TiO_2 NFs was determined with XRD patterns from the strongest peak (101) of anatase (JCPDS Card No. 00–021–1272) using Scherrer's equation (Fig. 4f). A mean value of 34 nm, 19 nm, and 18 nm was calculated for TiO_2 crystallites from samples containing 2 wt%, 4 wt%, and 8 wt% of Au, respectively. Some researchers found that noble metal NPs not only decrease the charge transfer of the composite TiO_2 NFs but can also act as conductive agents. This would contribute in reducing the TiO_2 particle size after the incorporation of noble metal NPs into TiO_2 NFs (Kim et al. 2010; Yang et al. 2013).

Through these results, it was demonstrated that TiO_2–Au composite NFs could be prepared with TiO_2 crystals with a tunable content of rutile and anatase. This mixture of TiO_2 phases helps to generate reactive oxygen species (Jingkun et al. 2008). Moreover, a presence of Au NPs with a size of about 10 nm should improve the photocatalysis properties of the TiO_2 NFs, as earlier demonstrated for samples of Au NPs in the size range of 3 ~ 30 nm (Murdoch et al. 2011). In this study, the photocatalytic properties of TiO_2 NFs with different phase ratio of anatase/rutile and TiO_2–Au composite NFs with Au size around 10 nm were investigated.

Photocatalytic activity

Effect of calcination temperature on TiO_2 NFs catalyst

Figure 5 shows the degradation rate toward MB dye using pristine TiO_2 NFs prepared under different calcination temperatures. From Fig. 5a, it can be clearly seen that after 10 min of photocatalytic reaction, the degradation level of TiO_2—500 °C reaches 82%, while it was only 65%, 27%, and 30% for TiO_2—600 °C, TiO_2—700 °C, and TiO_2—800°C catalysts respectively. The main phase of TiO_2—500 °C is anatase with an anatase to rutile ratio of 98:2. With a ratio of 84:16 for TiO_2—600 °C, a comparable photocatalytic performance to TiO_2—500 °C was measured after 20 min of irradiation, with the degradation level of around 92%, while it was

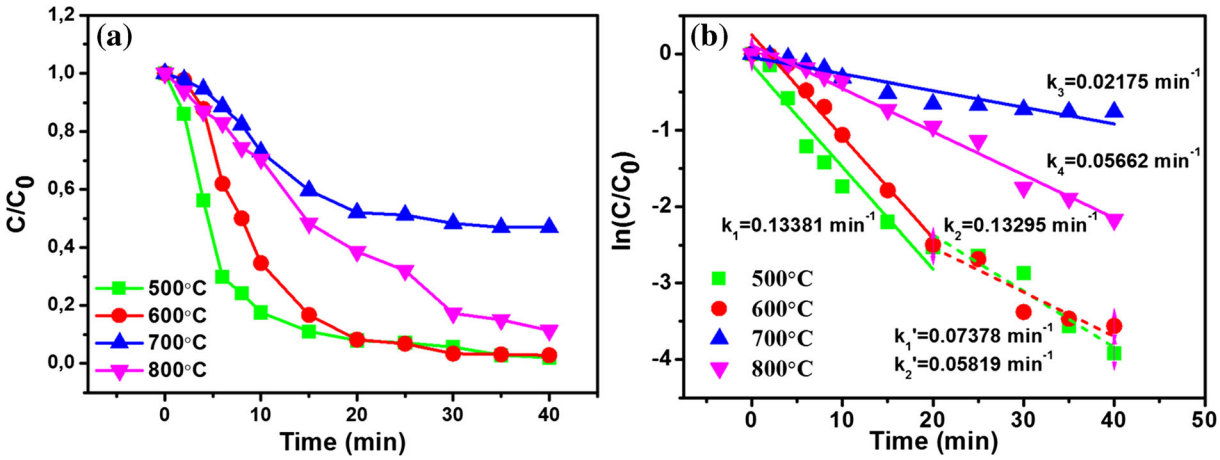

Fig. 5 **a** Variation of normalized C/C0 and **b** normalized ln(C/C0) of MB concentration as a function of UV light irradiation time for TiO_2 calcined at different temperatures

48% and 61% for catalyst of TiO_2—700 °C and TiO_2—800 °C, respectively. Within the first 20 min of reaction, dye concentration remained relatively important and the absorption and reaction rates of the dye on the catalyst was the critical factor, i.e., the turnover rate on the catalyst. Adsorption isotherms were carried out on different types of titanium-based P25, NFs, and nanotubes by Sara Cavaliere and her colleagues. They found that the best adsorption capacity was achieved by ES NFs, and increasing the buffer pH from 6 to 8 gave rise to the increase of adsorption capacity for P25 and ES NFs, due to the negative surface charge (Prelot et al. 2017). This was in good agreement with the zeta potential results and provided the strong evidence that the absorption and reaction rates influence the catalyst efficiency.

On the opposite, as photocatalysis process carries on, dye concentration is getting significantly lower, and the diffusion rate of the dye from the solution to the catalyst usually becomes a predominant contribution of the photocatalytic activity.

The photocatalytic efficiency could also be estimated based on the equation: $\ln(C/C_0) = -kt$, based on a pseudo-first-order kinetic, where k is the reaction rate constant, C/C_0 is the ratio of absorbance values corresponding to the characteristic peaks of different dyes before and after photocatalysis, and t is the reaction time (Salvador 2009). The reaction rate constant k is 0.02175 and 0.05662 min^{-1} for TiO_2—700 °C and TiO_2—800 °C, respectively. According to the results shown in Fig. 5a, the curves of TiO_2—500 °C and TiO_2—600 °C are close to each other with the parallel trend to the x-axis after 20 min. Thus, the kinetic also includes a slower decay, visible on Fig. 5b after 20 min. The reaction rate constant k was 0.13381 and 0.13295 min^{-1} within 20 min, while it became 0.07378 and 0.05819 min^{-1} after 20 min for TiO_2—500 °C and TiO_2—600 °C, respectively. The catalytic activity of TiO_2—500 °C NFs is superior to the one of the samples obtained for higher calcination temperatures. This could be explained by the fact that the calcination temperature can impact both the morphology and the anatase/rutile ratio of TiO_2. Indeed, the reaction rate is mainly related to the concentration of dye than the reaction activity sites of catalyst. The reaction rate is thus more limited by the concentration of remaining dyes in the solution.

Effect of Au contents on TiO_2–Au composite NFs catalyst

In order to evaluate the real photocatalytic performance of TiO_2–Au composite NFs with different Au contents, P25 commercial TiO_2 NPs catalyst from Degussa was used as a benchmark. P25 is widely used as a standard titania photocatalyst because of its high photocatalytic activity in many reaction systems (Shiraishi et al. 2013). As shown in Fig. 6a, the MB measured degradation with TiO_2–Au composite NFs catalyst was faster than the other catalysts, with a degradation level of 88% for TiO_2–Au—4 wt%, compared to 32% for P25 and 51% for TiO_2 NFs within an interval of 5 min. The performance of P25 and pristine TiO_2 NFs were very similar, with a total degradation time of 40 min and 35 min and the reaction rate constant k of 0.07865 min^{-1} and 0.07873 min^{-1}, respectively, while the total degradation

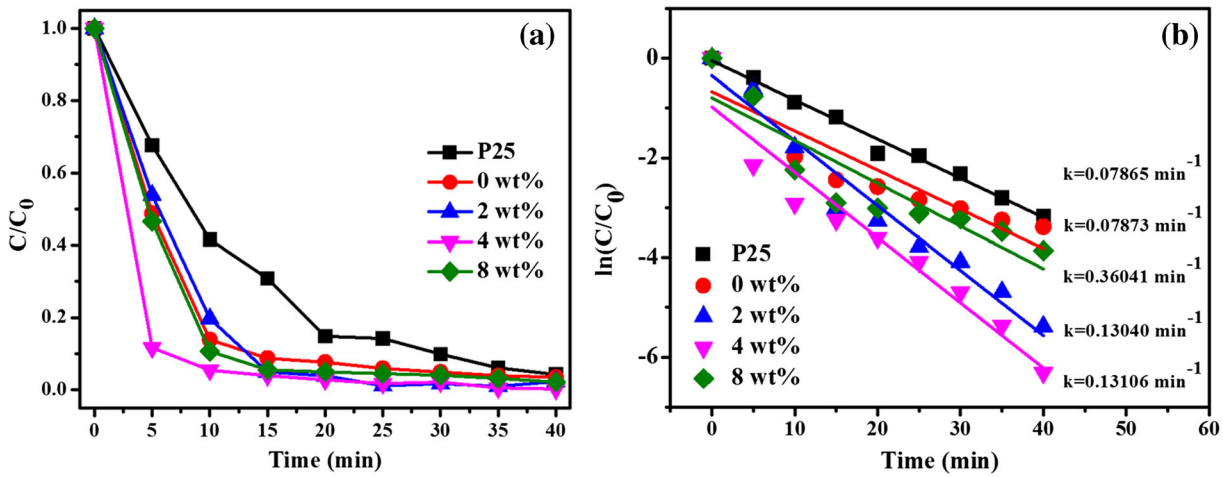

Fig. 6 **a** Variation of normalized C/C0 and **b** normalized ln(C/C0) of MB concentration as a function of UV light irradiation time for P25, TiO_2–Au composite NFs with different Au contents

time is only 15 min, with a reaction rate constant k of 0.13106 min^{-1}. It demonstrates that the morphology (NPs for P25 and NFs for TiO_2) or ratio of anatase/rutile (81:19 for P25 and 98:2 for TiO_2 NFs) is not necessarily a key parameter to enhance photocatalytic performances.

The catalytic activity of TiO_2–Au composite NFs was clearly enhanced by the presence of Au NPs. After 10 min, the degradation level of TiO_2–Au—4 wt% catalyst already reached 95%, compared to 80% for TiO_2–Au—2 wt% and 89% for TiO_2–Au—8 wt%. As the Au content increases, the number of Au NPs functionalizing TiO_2 increases, generating more active electron/hole pairs and increasing the total catalytic capacity (Murdoch et al. 2011). Au NPs are also strong UV absorbers and also act as recombination center to gather the e^-/h^+ pairs (Amato et al. 2018). When the Au NPs content exceeds a certain amount, the absorption from TiO_2 can be screened and thus lower the photoactivity of TiO_2–Au NFs. This balance between positive and negative effect of the addition of Au NPs is likely to explain why the catalytic activity for TiO_2–Au composite slightly decreases for the highest Au content. The TiO_2–Au NFs catalyst have good recyclability since it has only 1.4% of deactivation upon three recycling tests for the sample of TiO_2–Au–4 wt% (shown in SI Fig. 1).

The specific surface area is an important factor for catalysts, even if it is not the only influent factor determining the catalyst efficiency (Tian et al. 2014). The photocatalytic performance of TiO_2–Au composite NFs is better than P25, although their specific surface area (33 m^2 g^{-1}) measured by BET is smaller than that of P25 (50 m^2 g^{-1}). Those results confirm that the specific surface area cannot explain the better degradation activity measured with TiO_2–Au composite NFs than with P25 particles. The above-mentioned assumption, regarding the role played by the balance between the positive effect of increasing active sites and negative effect of e^-/h^+ pairs recombination with a raising Au amount, is thus strengthened (Table 3).

Effect of irradiation wavelength on TiO_2–Au composite NFs catalyst

As TiO_2 only absorbs light in the UV range, it has no activity in the visible range. It was important to check whether functionalization with Au NPs, by extending the absorption range to visible range, would induce photocatalytic enhancement by co-catalysis (Suljo et al. 2011). The sample with the best photocatalytic performance under UV irradiation, TiO_2–Au—4 wt% composite NFs, was chosen for photocatalysis experiments under irradiation with these different wavelengths, including 360 nm, 528 nm, and both 360 and 528 nm together. Comparing the results from Figs. 7a–c under irradiation with different wavelengths after 5 min, the TiO_2–Au composite NFs catalyst exhibits a degradation level of 48% at 360 nm, 12% at 528 nm, but up to 62% at 360 nm and 528 nm combined. After 30 min, the MB molecular degradation for experiments carried out under 360 nm and 528 nm reaches 96%, i.e., around 1.5 and 3 times faster than each wavelength used separately.

More details about the linear relationships between $\ln(C/C_0)$ and the reaction time (t) are shown in Fig. 7d.

Table 3 Specific surface area, crystallite size, and anatase/rutile ratio of P25, TiO_2, and TiO_2–Au—4 wt% composite NFs with different photocatalytic performances

Sample	Specific surface area $m^2\ g^{-1}$	Crystallite size nm	Anatase:rutile %	Reaction time min	Rate constant *k*
P25	50 ± 15	21	81:19	40	0.07865
TiO_2	17	27	98:2	35	0.07873
TiO_2–Au—4 wt%	33	19	98:2	15	0.13106

The catalytic reduction reactions confirm the pseudo-first-order kinetics. The reaction rate constant (k), calculated from the rate equation $\ln(C/C_0) = kt$, is 0.09796 min^{-1} for 360 nm and 528 nm, which is 3 times and 8.5 times higher than that for 360 nm (0.03223) and 528 nm (0.01152), respectively. When irradiating under 360 nm and 528 nm at the same time, the photocatalytic efficiency of TiO_2–Au catalyst improved compared to only UV or visible irradiation. For comparison, the reaction rate constant k is 0.01473 min^{-1} for pristine TiO_2 under 528 nm irradiation (see in SI Fig. 2) that is close to the reaction rate of TiO_2–Au catalyst (0.01152 min^{-1}) under 528-nm irradiation.

Photocatalytic mechanisms

The possible mechanism of photocatalytic degradation of MB over the optimal sample TiO_2–Au composite NFs under UV and visible irradiation is schematically illustrated in Fig. 8. Under UV light irradiation, TiO_2 generates photoexcited electron-hole pairs and the electrons (e^-) then transit from the valence band (VB) to the conduction band (CB). The Schottky barrier is formed with Au NPs to capture electrons, thus reducing the recombination rate of electron-hole pairs (Wang et al. 2018). Under visible light irradiation, the surface plasmon resonance effect (SPRE) of Au can promote the

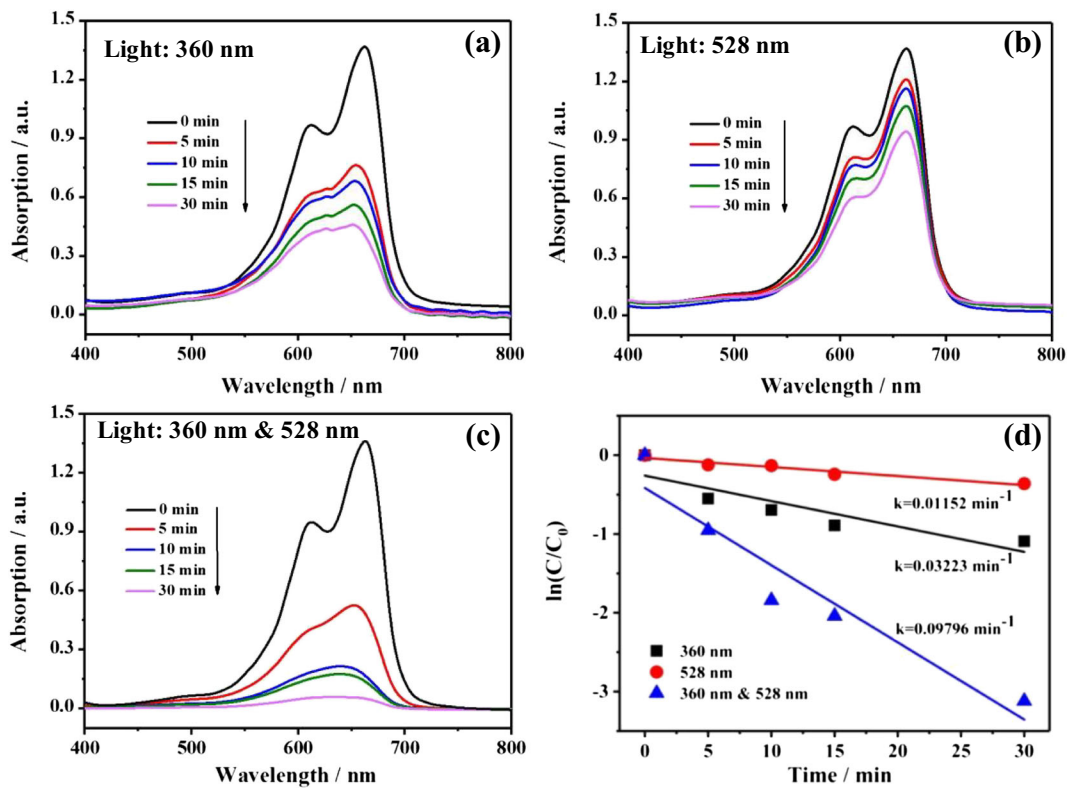

Fig. 7 UV–Vis absorption spectra of MB aqueous solution in photodegradation process under irradiation with different wavelengths in the presence of TiO_2–Au composite NFs: **a** 360 nm, **b** 528 nm, **c** 360 nm and 528 nm; **d** Variation of normalized ln(C/C0) of MB concentration as a function of time under irradiation with different wavelengths

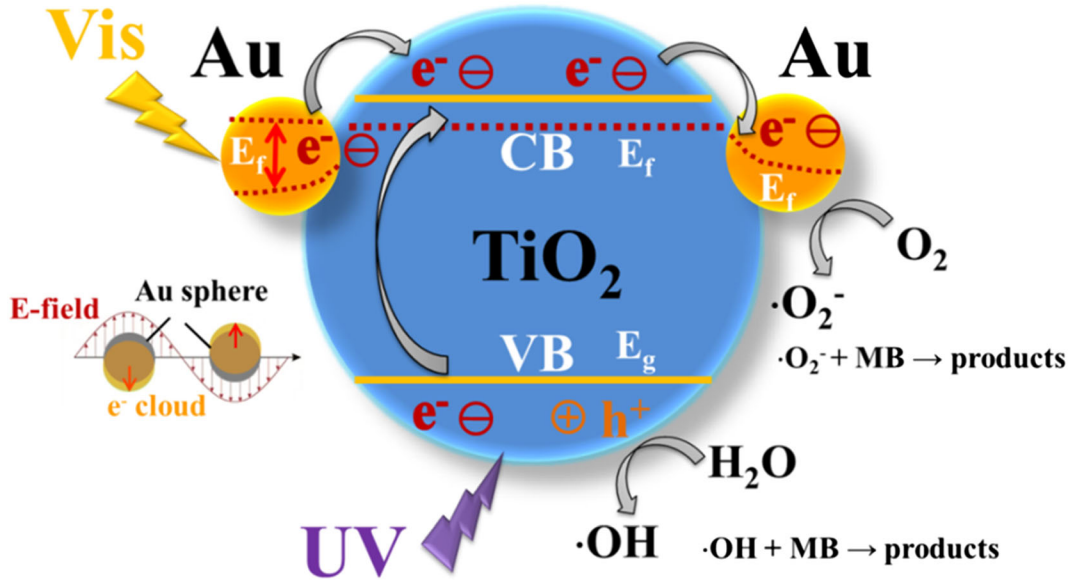

Fig. 8 Schematic diagram of the photocatalytic degradation of MB with TiO_2–Au composite NFs under UV and visible irradiation

absorption resonant photons with hot electrons generated by Au NPs to inject into the CB of TiO_2 (Tatsuma et al. 2017; Wang et al. 2018). Then the holes left in VB can produce hydroxyl radicals (OH·) by reaction with H_2O molecules (Online et al. 2017). In parallel, electrons (e^-) transfer to CB to react with the oxygen molecules (O_2) dissolved in the solution to yield superoxide radical anions ($\cdot O_2^-$). Those radicals (OH· and $\cdot O_2^-$) are strong oxidizing agents to decompose the organic dye (Mushtaq et al. 2016; Xia et al. 2017; Liu et al. 2019). As reported in the literature, the migration rate is very fast (less than 240 fs), thus the photogenerated h^+/e^- pairs can be effectively separated (Furube et al. 2007). Au NPs play two roles during the photocatalytic reaction process, one is as the generated electron (e^-) sink to decrease the recombination rate of e^-/h^+ and another one is more active to absorb the lower energy light in visible range to produce more charge carriers to enhance the light harvesting. Thus, combining the UV and visible irradiation together could improve the photocatalytic performance.

Conclusions

In summary, the thermal evolution of as-spun precursor composite NFs to reach pristine TiO_2 NFs and TiO_2–Au composite NFs was investigated in terms of morphology, structure, and phase composition, as well as their photocatalytic properties. The materials were produced by ES combined with subsequent calcination processes. The results indicated that the calcination temperature strongly affects the morphology and phase structures of titania. As the temperature increases, the content of anatase decreases while that of rutile increases in TiO_2. The ratio of anatase/rutile could be adjusted with the treatment temperature. TiO_2 NFs with a diameter around 164 nm and anatase/rutile ratio of 98:2 were fabricated at 500 °C and presented the best catalytic performances within 20 min, among all the samples.

Based on the photocatalytic performance achieved from TiO_2 NFs, TiO_2–Au composite NFs were synthesized with different Au contents. The TiO_2–Au—4 wt% catalyst with an average diameter of the NFs of about 171 nm and well-dispersed Au NPs (~ 10 nm) has the most interesting photocatalytic activity with a total degradation time of 15 min under UV irradiation, compared to 40 min and 35 min for P25 and pristine TiO_2 NFs, respectively. Under mixed wavelength irradiation, the TiO_2–Au catalyst reached a MB degradation level of 96%, after 30 min of irradiation, which is about 1.5 times faster than under 360 nm alone and 3 times faster than under 528 nm. It indicates that functionalization with Au NPs enhances the photocatalytic efficiency and appears as a key parameter to extend the absorption range from UV to visible. The photocatalytic mechanism involves the presence of Au and SPR excitation, inducing more active photogenerated excited e^-/h^+ pairs

and limiting their recombination. The $\cdot O_2^-$ and OH· radicals are effective species for the degradation of MB. The overall results demonstrate the importance of optimization of calcination temperature on TiO_2 phase composition and the influence of Au contents for photocatalysis performances. Fabrication of Au functionalized TiO_2 NFs by ES is a simple, controllable, and efficient approach with great interest for environment-related applications.

Acknowledgments The authors thank Dr. Ing. Rodica Chiriac of the Ingénieur d'études CNRS for the assistance with the BET measurements, Dr. Bruno Gardiola from Laboratoire Multimatériaux & Interfaces (LMI) for the assistance with calculation of the ratio anatase/rutile by software BASS, and PhD Ylane Malicet from Laboratoire Multimatériaux & Interfaces (LMI) for the assistance with ICP measurements. Finally, authors would like to acknowledge the CTμ (Centre Technologique des Microstructures, microscopies.univ-lyon1.fr) for the access to the SEM and TEM microscopes used in this work.

Funding information This work was supported by National Natural Science Foundation of China (Grant No. 51702224), Sichuan Province Science and Technology Project (Grant No. 2017GZ0416), and the program of Postdoctoral Science Foundation of Sichuan University (Grant No. 2018SCU12001).

Compliance with ethical standards

Conflict of interest The authors declare that they have no conflict of interest.

References

Amato CAD, Giovannetti R, Zannotti M, Rommozzi E, Ferraro S, Seghetti C, Minicucci M (2018) Enhancement of visible–light photoactivity by polypropylene coated plasmonic Au/TiO_2 for dye degradation in water solution. Appl Surf Sci 441:575–587. https://doi.org/10.1016/j.apsusc.2018.01.290

Bian Z, Tachikawa T, Zhang P, Fujitsuka M, Majima T (2014) Au/TiO_2 superstructure–based plasmonic photocatalysts exhibiting efficient charge separation and unprecedented activity. J Am Chem Soc 136:458–465. https://doi.org/10.1021/ja410994f

Butburee T, Bai Y, Wang H, Chen H, Wang Z, Liu G, Zou J, Khemthong P, Qing G, Lu M, Wang L (2018) 2D Porous TiO_2 single–crystalline nanostructure demonstrating high photo–electrochemical water splitting performance. Adv Mater 30:1–8. https://doi.org/10.1002/adma.201705666

Cavaliere S, Subianto S, Chevallier LJ, Jones D, Roziere J (2011) Single step elaboration of size-tuned Pt loaded titania nanofibres. Chem Commun 47:6843–6836. https://doi.org/10.1039/C1CC11716E

Chen X, Liu L, Yu P, Mao S (2011) Increasing solar absorption for photocatalysis with black hydrogenated titanium dioxide nanocrystals. Science 331:746–750. https://doi.org/10.1126/science.1200448

Conceicao DS, Vieira Ferreira LF (2018) Photochemical behavior of Ag^0 or Au^0 decorated nanostructured TiO_2 prepared by a facile in situ reduction method. Chemistry Select 3:773–778. https://doi.org/10.1002/slct.201702165

Dambournet D, Belharouak I, Amine K (2010) Tailored preparation methods of TiO_2 anatase, rutile, brookite: mechanism of formation and electrochemical properties. Chem Mater 22:1173–1179. https://doi.org/10.1021/cm902613h

Fazio G, Ferrighi L, Di C (2016) Photoexcited carriers recombination and trapping in spherical vs faceted TiO_2 nanoparticles. Nano Energy 27:673–689. https://doi.org/10.1016/j.nanoen.2016.08.003

Furube A, Du L, Hara K, Katoh R, Tachiya M (2007) Ultrafast plasmon–induced electron transfer from gold nanodots into TiO_2 nanoparticles. J Am Chem Soc 129:14852–14853. https://doi.org/10.1021/ja076134v

Greiner A, Wendorff JH (2007) Electrospinning: a fascinating method for the preparation of ultrathin fibers. Angewandte Chemie–International Edition 46:5670–5703. https://doi.org/10.1002/anie.200604646

Hahn H, Logas J, Averback RS (1990) Sintering characteristics of nanocrystalline TiO_2. J Mater Res 5(3):609–614. https://doi.org/10.1557/JMR.1990.0609

Han E, Vijayarangamuthu K, Youn J, Park YK, Jung SC, Jeon KJ (2018) Degussa P25 TiO_2 modified with H_2O_2 under microwave treatment to enhance photocatalytic properties. Catal Today 303:305–312. https://doi.org/10.1016/j.cattod.2017.08.057

Ho J, Kang M, Choung S, Ogino K, Miyata S, Kim M, Park J, Kim J (2004) The preparation of TiO_2 nanometer photocatalyst film by a hydrothermal method and its sterilization performance for Giardia lamblia. Water Res 38:713–719. https://doi.org/10.1016/j.watres.2003.10.011

Jingkun J, Günter O, Alison E, Robert G, Pamela M, Pratim B (2008) Does nanoparticle activity depend upon size and crystal phase? Nanotoxicology 2(1):33–42. https://doi.org/10.1080/17435390701882478

Lang X, Chen X, Zhao J (2014) Heterogeneous visible light photocatalysis for selective organic transformations. Chem Soc Rev 43:473–486. https://doi.org/10.1039/C3CS60188A

Li D, Xia Y (2003) Fabrication of titania nanofibers by electrospinning. Nano Lett 3:555–560. https://doi.org/10.1021/nl034039o

Liu B, Wang J, Yang J, Zhao X (2019) Charge carrier interfacial transfer pathways from TiO_2 and Au/TiO_2nanorod arrays to electrolyte and the association with photocatalysis. Appl Surf Sci 464:367–375. https://doi.org/10.1016/j.apsusc.2018.09.031

Lyulyukin MN, Kolinko PA, Selishchev DS, Kozlov DV (2018) Hygienic aspects of TiO_2–mediated photocatalytic oxidation of volatile organic compounds: air purification analysis using a total hazard index. Appl Catal B Environ 220:386–396. https://doi.org/10.1016/j.apcatb.2017.08.020

Moretti E, Rodríguez–aguado E, Molina AI, Rodríguez–castellón E, Talon A, Storaro L (2018) Sustainable photo–assisted CO oxidation in H_2–rich stream by simulated solar light response

of Au nanoparticles supported on TiO_2. Catal Today 304: 135–142. https://doi.org/10.1016/j.cattod.2017.09.048

Murdoch M, Waterhouse GIN, Nadeem MA, Metson JB, Keane MA, Howe RF, Llorca J, Idriss H (2011) The effect of gold loading and particle size on photocatalytic hydrogen production from ethanol over Au/TiO_2 nanoparticles. Nat Chem 3(6):489–492. https://doi.org/10.1038/NCHEM.1048

Mushtaq F, Asani A, Hoop M, Chen X, Ahmed D, Nelson BJ, Pané S (2016) Highly efficient coaxial TiO_2–Pt/Pd tubular nanomachines for photocatalytic water purification with multiple locomotion strategies. Adv Funct Mater 26:6995–7002. https://doi.org/10.1002/adfm.201602315

Online VA, Arshad MS, Kovac J (2017) Determination of Schottky barrier height and enhanced photoelectron generation in novel conversion applications. J Mater Chem C 5: 10509–10516. https://doi.org/10.1039/C7TC02633A

Online VA, Zhang Z, Li A, Cao S, Bosman M, Li S, Xue C (2014) Direct evidence of plasmon enhancement on photocatalytic hydrogen generation overAu/Pt–decorated TiO_2 nanofibers. Nanoscale 6:5217–5222. https://doi.org/10.1039/C3NR06562F

Salvador P (2009) The direct–indirect kinetic model in photocatalysis: a reanalysis of phenol and formic acid degradation rate dependence on photon flow and concentration in TiO_2 aqueous dispersions. Appl Catal B Environ 88:50–58. https://doi.org/10.1016/j.apcatb.2008.09.035

Shim CS, Kim H, Patil PS, Hong CK (2016) In situ processed gold nanoparticle–embedded TiO_2 nanofibers enabling plasmonic perovskite solar cells to exceed 14% conversion efficiency. Nanoscale 8:2664–2677. https://doi.org/10.1039/C5NR07395B

Shiraishi Y, Hirakawa H, Togawa Y, Sugano Y, Ichikawa S, Hirai T (2013) Rutile crystallites isolated from Degussa (Evonik) P25 TiO_2: highly efficient photocatalyst for chemoselective hydrogenation of nitroaromatics. ACS Catal 3:2318–2326. https://doi.org/10.1021/cs400532p

Sridhar V, Park B, Sitti M (2018) Light–driven janus hollow mesoporous TiO_2–Au microswimmers. Adv Funct Mater 28:1704902. https://doi.org/10.1002/adfm.201704902

Su R, Tiruvalam R, He Q, Dimitratos N, Kesavan L, Hammond C, Lopez–sanchez JA, Bechstein R, Kiely CJ, Hutchings GJ, Besenbacher F (2012) Promotion of phenol photodecomposition over TiO_2 using Au, Pd, and Au–Pd nanoparticles. ACS Nano 6:6284–6292. https://doi.org/10.1021/nn301718v

Suljo L, Phillip C, David BI (2011) Plasmonic-metal nanostructures for efficient conversion of solar to chemical energy. Nat Mater 10(12):911–921. https://doi.org/10.1038/NMAT3151

Tatsuma T, Nishi H, Ishida T (2017) Plasmon-induced charge separation: chemistry and wide applications. Chem Sci 8(5):3325–3337. https://doi.org/10.1039/C7SC00031F

Tian J, Zhao Z, Kumar A, Boughton I, Liu H (2014) Recent progress in design, synthesis, and applications of one–dimensional TiO_2 nanostructured surface heterostructures: a review. Chem Soc Rev 43:6920–6937. https://doi.org/10.1039/C4CS00180J

Tsukamoto D, Shiraishi Y, Sugano Y, Ichikawa S, Tanaka S, Hirai T (2012) Gold nanoparticles located at the interface of anatase/rutile TiO_2 particles as active plasmonic photocatalysts for aerobic oxidation. J Am Chem Soc 134: 6309–6315. https://doi.org/10.1021/ja2120647

Wang T, Zhang Y, Wang Y, Wei J, Zhou M, Zhang Z, Chen Q (2018) One-step electrospinning method to prepare gold decorated on TiO_2 nanofibers with enhanced photocatalytic activity. J Nanosci Nanotechnol 18:3176–3184. https://doi.org/10.1166/jnn.2018.14543

Xia H, Wu S, Bi J, Zhang S (2017) Controlled preparation of M (Ag, Au)/TiO_2 through sulfydryl–assisted method for enhanced photocatalysis. Nanotechnology 28:465604. https://doi.org/10.1088/1361-6528/aa8d94

Xing M, Zhou Y, Dong C, Cai L, Zeng L, Shen B, Pan L, Dong C, Chai Y, Zhang J, Yin Y (2018) Modulation of the reduction potential of TiO_2−x by fluorination for efficient and selective CH_4 generation from CO_2 photoreduction. Nano Lett 18: 3384–3390. https://doi.org/10.1021/acs.nanolett.8b00197

Xiong Y, Washio I, Chen J, Cai H, Li Z, Xia Y (2006) Poly (vinyl pyrrolidone): a dual functional reductant and stabilizer for the facile synthesis of noble metal nanoplates in aqueous solutions. Langmuir 22:8563–8570. https://doi.org/10.1021/la061323x

Yan J, Zhang X, Akita T, Haruta M, Xu Q (2010) One–step seeding growth of magnetically recyclable Au@Co core–shell nanoparticles: highly efficient catalyst for hydrolytic dehydrogenation of ammonia borane. J Am Chem Soc 132: 5326–5327. https://doi.org/10.1021/ja910513h

Yang J, Mou C (2018) Ordered mesoporous Au/TiO_2 nanospheres for solvent–free visible–light–driven plasmonic oxidative coupling reactions of amines. Appl Catal B Environ 231: 283–291. https://doi.org/10.1016/j.apcatb.2018.02.054

Yang X, Fu H, Wong K, Jiang X, Yu A (2013) Hybrid Ag@TiO_2 core-shell nanostructures with highly enhanced photocatalytic performance. Nanotechnology 24(41):1–10. https://doi.org/10.1088/0957-4484/24/41/415601